Progress in Medical Devices
eISSN: 2957-5478

Zentime

Research Article https://doi.org/10.61189/780603itrglq

Precision cooling radiofrequency ablation under tumor boundary temperature control

Ruiyan Qian, Haixiao Lin, Dandan Gu, Difang Liu, Haitao Yao, Danni Rui, Yu Zhou

School of Health Sciences and Engineering, University of Shanghai for Science and Technology, Shanghai 200093, China.

Declaration of conflict of interest: None.

Received June 8, 2023; Accepted August 28, 2023; Published September 30, 2023

Highlights

- The outcomes derived from simulation and ex vivo experiments exhibit precise control over the range of radiofrequency ablation when employing boundary temperature control.
- It was observed in this study that a single ablation procedure can achieve an ablation diameter of up to 30 mm.
- The regular index and elliptic index of the radiofrequency ablation area tend to be a spherical shape, which holds potential benefits for the radiofrequency ablation surgeries.

Abstract

Radiofrequency ablation (RFA) represents a convenient, minimally invasive, and cost-effective approach for the treatment of small liver cancers measuring less than 3 cm in diameter. Nonetheless, the existing RFA techniques encounter challenges in precisely controlling the extent of ablation and the risk of overheating, which can lead to damage on the surrounding tissues. The ability to control the ablation area also plays a crucial role in the success of RFA procedures. To address these issues, we introduce a novel method that utilizes tumor boundary temperature monitoring to achieve precise control over the RFA process. Through the utilization of COMSOL Multiphysics simulation software, the proposed method was verified by comprehensive simulation and modeling and its efficacy in achieving regional control was testified. Subsequently, ex vivo experiments were conducted employing a custom-designed cooling RFA instrument. The experimental results demonstrated that the RFA controlled by boundary temperature yielded an ablation area with a diameter approaching 30 mm. In comparison to the standard spherical solidification zone (characterized by both the ellipticity and regularity indices of 1), the cooling RFA discoloration zone, under boundary temperature control, exhibited a maximum deviation of 7% in the ellipticity index and 17% in the regularity index. The average ellipticity index was determined to be 0.96, while the average regularity index was 0.86. Collectively, these findings underscore the capability of the proposed temperature-controlled cooling RFA method to attain precise control over the ablation area, contributing to comprehensive ablation of tumor tissue within the target region.

Keywords: Cooling radiofrequency ablation, simulation, temperature controlled, regional control

Introduction

Cancer is one of the leading causes of death globally [1]. To effectively improve patient well-being, cancer treatment technologies have constantly been advancing. Radiofrequency ablation (RFA) has emerged as a safe and effective treatment method that plays a vital role in combating cancer [2]. RFA utilizes radiofrequency energy to generate thermal effects in tumor tissues, resulting in coagulation necrosis and the successful treatment of diseased tissues [3]. It is suggested that when the tumor cells are exposed to temperatures exceeding 42 °C, their biochemical reactions and metabolic processes become disrupted. Cell apoptosis is observed within 8 minutes at 46 °C, and in just 2 minutes at 51 °C. Temperature surpassing 60 °C can prompt rapid protein denaturation and necrosis within the cells, while temperature exceeding 100 °C can result in cell water boiling, leading to tissue gasification or carbonization [4, 5]. To achieve complete coagulation and necrosis of tumor tissues, the traditional multi-polar RFA technique employed in the treatment of small- and medium-sized liver cancers often leads to tissue carbonization, reducing tissue conductivity and hindering

Address correspondence to: Yu Zhou, School of Health Sciences and Engineering, University of Shanghai for Science and Technology, No.516 Jungong Road, Shanghai 200093, China. Tel: 18021042556, E-mail: zhouyu_working@163.com.

the transfer of radiofrequency energy to distant lesions. The use of unipolar RFA requires multiple ablations, which faces technical challenges, such as the determination of the optimal number of ablations and the precise placement of the electrodes [6]. While expanding the ablation range is important, precise control of the ablation range remains a significant challenge in current radiofrequency therapy.

In response to these challenges, cooling RFA (CRFA) has emerged as a promising technology. The safety of CRFA is comparable to that of traditional RFA [7]. Nevertheless, in comparison to conventional approaches, CRFA confers a multitude of advantages [8]. By effectively reducing the contact temperature between electrodes and tissues, CRFA mitigates the risk of tissue carbonization or gasification, expands the ablation range, and improves the therapeutic effect on liver cancer [9]. CRFA introduces cooling functionality to the existing RFA technology by incorporating a cooling device into the electrode needle. Some attempts have been made to expand the ablation range by regulating CRFA output through impedance control. However, these methods often result in irregular ablation areas and pose risks to healthy tissues [10].

In order to expand the ablation range, reduce treatment frequency, and optimize patients' treatment experience, this study introduces an independently developed CRFA system. Meanwhile, in order to enhance the precision of ablation range in clinical practice, mitigate the risk of injury to healthy tissues, and maximize the safety of patients, a novel tumor boundary temperature-controlled ablation algorithm is proposed. The power output of RFA is controlled based on the tumor boundary temperature, which is monitored in real-time to achieve more regular and precise ablation range. This study employed the multi-physics simulation software COMSOL to model the physical phenomena of RFA under boundary temperature control. Furthermore, ex vivo experiments were conducted using a self-developed CRFA device to analyze and evaluate the RFA outcomes under boundary temperature control, so as to verify the effectiveness of the algorithm.

Material and Methods

CRFA mathematical model

The main idea of supplying electric current in the tumor area is to convert the electrical energy into thermal energy according to the law of conservation of energy. The primary mechanism of energy propagation takes place through electrical conduction, which can be mathematically characterized as a coupled phenomenon involving quasi-static conduction and thermal conduction. The mathematical representation of the governing equation for the current interface can be expressed as Equation 4.1.

$$-\nabla(\sigma\nabla V - J^e) = Q_j \tag{4.1}$$

where σ is the electrical conductivity (S/m), J^e is an externally generated current density (A/m^2), and Q_j is the current source (A/m^3). In the CRFA model, there are no other applied current sources other than the electrodes. J^e and Q_j are zero, substituting these values to simplify the electric field distribution in the CRFA model, as shown in Equation 4.2 [11].

$$-\nabla(\sigma\nabla V) = 0 \tag{4.2}$$

The bio-heat transfer equation employed is the classical Pennes bio-heat transfer equation [12]. This heat transfer equation is often used in biomedical engineering to simulate hyperthermia for cancer treatment, which is described as follow:

$$\rho c\frac{\partial T}{\partial t} = \nabla\cdot(k\nabla T) - \rho_b c_b \omega_b (T - T_b) + Q_m + Q_{hs} \tag{4.3}$$

where ρ and ρ_b are the density of tissue and blood, respectively (kg/ m^3), c and c_b are the specific heat capacity of tissue and blood, respectively (J/kg · °C), T and T_b are the temperatures of tissue and blood (°C), ω_b is the volume blood perfusion rate (s^{-1}), Q_m is the metabolic heat generation rate of tissue metabolic processes (W/m^3), and Q_{hs} is the heat generated by the electrodes of the RFA device (W/m^3).

CRFA incorporates a cooling water circulation system to cool the electrode needle, thereby engaging both solid and fluid heat transfer phenomena. The fluid heat transfer component encompasses the convection and heat conduction processes within the cooling water, while the solid heat transfer pertains to the heat transfer mechanism occurring within the electrode needle tube. The heat exchange between the fluid cooling water and the solid electrode needle is mathematically modeled using a fluid-solid coupling equation:

$$\rho c\frac{\partial T}{\partial t} + \rho c_p u\nabla T + \nabla q = Q \tag{4.4}$$

$$q = -k\nabla T \tag{4.5}$$

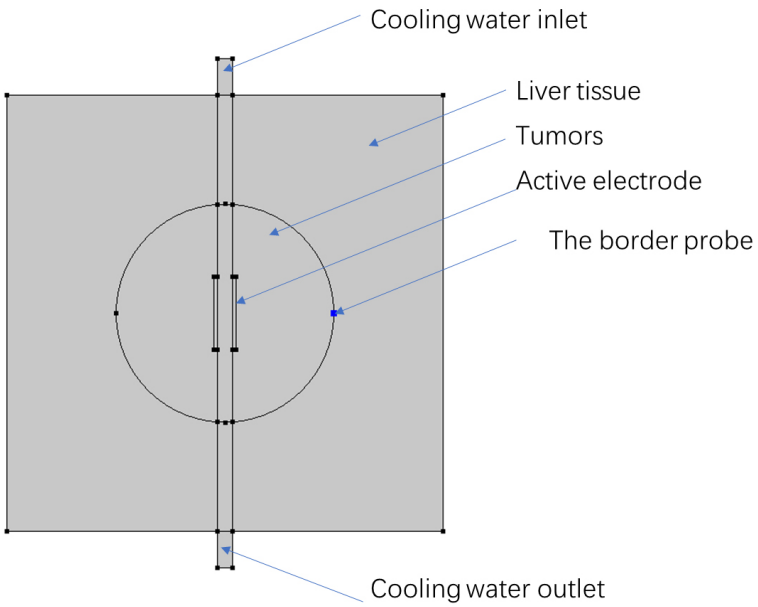

Figure 1. 2D geometry of the CRFA. CRFA, cooling radiofrequency ablation.

where $\rho c\frac{\partial T}{\partial t}$ is the transient term, $\rho c_p u\nabla T$ is the convection term, ρ is the electrode needle density (g/cm^3), c_p is the specific heat capacity of the substance (J/kg · °C), T is the temperature field (°C), u is theflow rate field of cooling water (m/s), ∇q is the diffusion term, Q is the heat source term (W), k is the thermal conductivity, and ∇T is the temperature difference (°C).

At each time step, the cumulative damage integral is computed using the well-established Arrhenius equation:

$$\Omega(t)=\ln\frac{c(0)}{c(t)}=A\int_0^T e^{-\Delta E/RT(t)}dt \qquad (4.6)$$

where c(t) is the concentration of living cells, R is the universal gas constant, A is a "frequency" factor for the kinetic expression (s^{-1}), and ΔE is the activation energy for the irreversible damage reaction (J/mol). During the finite element simulation of tissue damage, the critical threshold of the damage integral, denoted as Ω=1, corresponds to a 63% probability of cellular demise at a specific spatial location. Consequently, when the level of damage surpasses the 63% threshold, cell damage within the tissue reaches a critical threshold, resulting in the coagulation of the tissue and cessation of tissue perfusion [13].

The mathematical representation of the temperature dependency of electrical and thermal conductivity frequently employed in computational modeling of RFA can be approximated by a growth rate of +2% below the temperature threshold of 100 °C. However, once the temperature exceeds 100 °C, the effect of dehydration on the conductivity can be expressed by employing a sudden decrease of two or four orders of magnitude, while maintaining a constant value for thermal conductivity [14]. Consequently, in the context of modeling CRFA, a linear rate of change of -2%/°C for impedance was adopted, as outlined in Conway's investigation, to establish the mathematical function of impedance, denoted as R (T) [15].

$$R(T)=\begin{cases}R_0[1-(T-T_0)\times 2\%] & T<100℃\\ 1700 & T>100℃\end{cases} \qquad (4.6)$$

Establishment of the CRFA geometric model

In this study, the application of CRFA in the treatment of liver tumors involved the insertion of an active electrode into the tumor tissue for current delivery. Numerical simulations based on the theoretical model of the RFA process were developed to depict the corresponding geometry. As depicted in **Figure 1**, the model consisted of a circular region representing the liver tumor tissue, where the tumor size could be adjusted by controlling its diameter. The simulated RFA targeted tumors with diameters of 30 mm or less. The square area symbolized healthy liver tissue and possessed dimensions of 60 mm×60 mm. The electrode needle tube had a diameter of 2 mm and a length of 70 mm. The central part of the electrode, connected to the tumor center, functioned as the active electrode, while the remaining portion was electrically insulated. The active electrode itself had a diameter of 2 mm and a length of 10 mm. To monitor the temperature of the tumor boundary and the extent of necrotic tissue, a boundary probe was incorporated.

Considering the typical round or oval shape of tumor tissues, the ground pad in clinical practice is usually positioned at a considerable distance from the active electrode to ensure a uniform current distribution from the active electrode outward. As the ex vivo experiments exhibited axial symmetry in terms of geometry,

Table 1. Values of physical constants

Tissue Density	ρ=1060（kg/m^3）
Thermal conductivity	0.5020（W/K·m）
Tissue heat capacity	c=3600（J/kg·K）
Tissue electrical conductivity	σ=0.148(S/m)
Blood density	ρ_b= 1000(kg/m^3)
Blood heat capacity	c_b=4180（J/kg·K）
Perfusion coefficient	ω_b=6.4e^{-3}(s^{-1})

the CRFA simulation was simplified as a 2D model to significantly reduce the computational burden. The overall model closely resembled the insertion of a hollow electrode needle into the central region of liver tissue, with only the active electrode being electrically active as the current conductor while cooling water flowed through the interior of the electrode needle conduit. The top of the electrode needle served as the cooling water inlet, while the bottom functioned as the outlet.

Regarding the initial conditions of the model, the electrically insulating boundary conditions were applied to the nonconducting section of the electrode needle, and the four sides of the liver tissue were set to the ground state. The initial voltage of the entire simulation model was set to 0 V, while the cooling water temperature was maintained constant at 20 °C. Since the room temperature during the ex vivo experiments was approximately 23 °C, the initial tissue temperature was set to 23 °C.

The values of the individual physical constants are listed in **Table 1** [16].

The simulation was performed using COMSOL Multiphysics software. The radiofrequency output was controlled by monitoring the temperature at the tumor boundary using a probe. The observed ablation results were analyzed and evaluated. A bovine liver was used as the experimental subject, and a negative plate were affixed to the lateral side of the bovine liver, while a positioning plate was positioned directly above the bovine liver. The electrode needle was carefully inserted into the bovine liver via the central aperture of the positioning plate. Four temperature-measuring needles were introduced through the small aperture on the positioning plate, maintaining a distance of 15 mm from the central aperture. The thermocouple-based temperature measuring points were situated at the same depth as the exposed segment of the electrode needle. The radiofrequency energy generator operated in a constant power mode, and the experimental setup employed a cooling needle electrode measuring 2 mm in diameter and 250 mm in length, with a 15 mm bare leakage and uninsulated segment. The output duration was set to 900 s, and a total of five experimental iterations were conducted to document the size of the ablation area and the temperature within the ablation zone. The experimental protocol entailed activating the cooling apparatus. Once the cooling fluid reached the target temperature, the ex vivo CRFA procedure was initiated. Throughout the experiment, adaptive power output was realized by the control algorithm.

Development of the CRFA system

The design of the CRFA device necessitates adherence to the control algorithm's parameters, which involve temperature detection of biological tissue and adjustment of the output power based on impedance information. Therefore, the device must incorporate the corresponding circuitry to accurately detect temperature and impedance information, so as to ensure minimal errors and compliance with industry standards. Additionally, stable closed-loop control is essential, with impedance and temperature information serving as feedback variables to regulate the magnitude of radiofrequency energy and ensure controllable output power.

Following the design requirements, the hardware circuitry of the CRFA device primarily consists of the human-computer interaction interface, the main control module, the power supply module, the radiofrequency power amplifier module, and the interface module. External components include the electrode needle, temperature measuring needle, and negative electrode plate, as illustrated in **Figure 2A**. The human-machine interface comprises a programmable touch capacitive screen capable of displaying the operational status, by which users can select the output mode and control the device's switch. The power supply module furnishes power to the entire hardware system by initially converting 220 V alternating current to 48 V direct current (DC), which is then adjustable from 0-70 V DC to provide energy for the radiofrequency power amplifier. The main control module employs the STM32F103RCT6 MCU to oversee intelligent algorithm operations, power module control, output parameter control, temperature and impedance information detection, and other functions. Simultaneously, the 48 V DC output of power module can be further converted to 12 V, 3.3 V, and 8 V DC to accommodate the equipment control and detection sections. The radiofrequency power amplifier module incorporates a symmetric class E power amplifier that transforms the adjust-

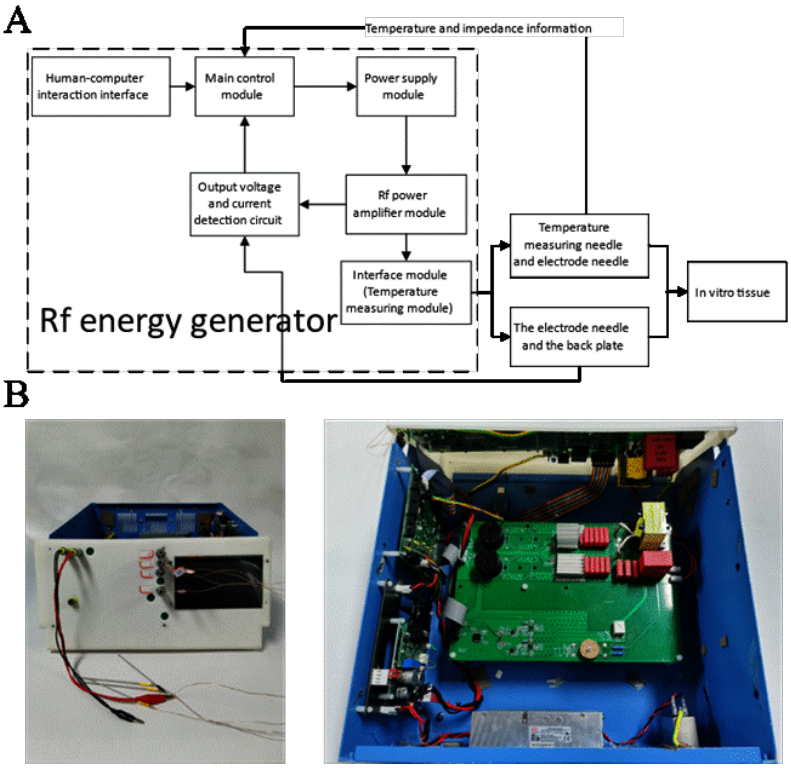

Figure 2. CRFA device. (A) Structure block diagram; (B) Appearance of the CRFA device. RF, radiofrequency; CRFA, cooling radiofrequency ablation.

able DC output from the power supply module into alternating current radiofrequency energy through a resonant circuit. The voltage and current detection circuit captures the voltage and current outputs of the radiofrequency power amplifier and converts them into low-voltage signals, proportionally feeding them back to the main control module. The interface module includes a temperature measuring circuit, a negative plate detection circuit, and an isolation transformer. The temperature measuring circuit amplifies the analog signals acquired by the temperature measuring needle and feeds them back to the main control module, while the negative plate detection circuit verifies the proper alignment of the negative plate with the human body. The isolation transformer ensures electrical isolation between the application and intermediate parts and is connected to the radiofrequency power amplifier, with its secondary side linked to the electrode needle and negative plate. During operation, radiofrequency current flows between the negative plate and the electrode needle, and real-time tissue temperature is collected using a K-type thermocouple. The overall appearance diagram and internal structure of the device are presented in **Figure 2B**.

Figure 3A presents the structural diagram of the cooling equipment, delineating the constituent elements such as the water pump, the refrigeration device, the radiator water discharge, and the control module. These components collaboratively facilitate the operation of the cooling system, enabling the circulation and cooling of the coolant. The primary objective of this cooling equipment is to effectively mitigate the elevated temperature of the electrode needle by dissipating heat through the coolant circulation process. **Figure 3B** shows the actual appearance of the water-cooling device.

Algorithm design and mechanism

The cooling apparatus facilitates the infusion of coolant into the electrode needle, thereby establishing a circulating mechanism for cooling the radiofrequency electrode. This mechanism effectively delays the onset of overheating and tissue carbonization. To further augment the cooling efficacy while ensuring uniform ablation, an enhanced output mode of radiofrequency energy was implemented, incorporating a duty cycle lasting 15 minutes. Within each cycle, the delivery of radiofrequency energy was sustained for 50% of the time, with the remaining 50% of the time allocated for output cessation. Additionally, the utilization of backflowing tissue fluid allows for the propagation of radiofrequency energy to more distal regions from the electrode [17].

The regional control algorithm plays a crucial role in governing the activation and power output of the system, responding to variations in tissue impedance and temperature. This dynamic regulation helps to prevent eschar formation near the electrode needle while ensuring compliance with the ablation area standard. The dimensions of the ablation zone are primarily dictated by the spatial separation between the temperature-measuring needle and the electrode needle.

Figure 4 provides a visual representation in the form of a flowchart, illustrating the process of power adjustment during radiofrequency en-

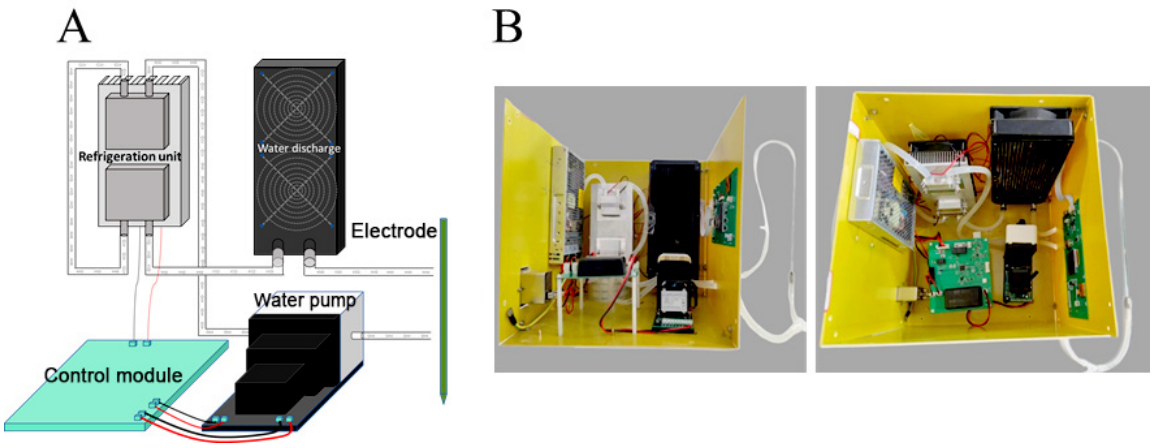

Figure 3. Schematic diagram of cooling equipment. (A) Structure; (B) Appearance of the cooling equipment.

ergy output based on impedance information. The initial cellular composition comprises the cell membrane and intracellular fluid, while extracellular fluid and intercellular stroma encompass the cellular structure. Upon introduction of an excitation current into the biological tissue, the current follows various pathways, bypassing the cells. Predominantly, the current flows within the extracellular fluid, with a fraction penetrating the cell membrane and permeating the intracellular fluid [18]. Ablation is conducted at higher power levels, resulting in cell destruction as the temperature rises, accompanied by fluid outflow from the tissue. Consequently, the tissue impedance progressively diminishes from a relatively high value to a minimum value, stabilizing for a certain duration. During this stable period, the administration of high-power energy does not induce tissue overheating. Excessive ablation boundary temperatures can inflict unwarranted thermal damage to neighboring tissues or blood vessels. Hence, the algorithm continuously monitors the real-time ablation boundary temperature recorded by the temperature-measuring needle. If the temperature exceeds 60 °C, the device halts the output and awaits tissue to cooldown. Simultaneously, when the device output is stopped, the reflux of tissue fluid reduces impedance near the electrode needle, facilitating the formation of a larger ablation area during subsequent heating and ensuring control over the ablation area size. Radiofrequency energy output continues when the boundary temperature is below 51 °C.

Methods for evaluating the effect of CRFA ex vivo

RFA involves the utilization of high-frequency alternating current, typically within the frequency range of 375-500 kHz. The radiofrequency applicators, referred to as electrodes, can be categorized as monopolar electrodes with a single active electrode applicator, where current dissipation occurs at one or more negative plates [19]. By delivering this energy through the electrodes into the patient's tissues, heating and subsequent destruction of the targeted tissue are achieved through variations in tissue conductivity. Radiofrequency electrodes generate an alternating electric field, leading to the oscillation of ions within the targeted tissue and the generation of heat. Consequently, cellular protein denaturation occurs, resulting in the loss of cellular viability [20, 21].

When monopolar RFA is utilized for tumor ablation in organs such as the liver, kidney, heart, and prostate, the evaluation of the CRFA takes place after the diseased tissue being coagulated. Complete and uniform destruction of cellular structures is observed within the pale region of the ablated lesion tissue, while the surrounding normal tissue exhibits a dark red appearance [22]. Several studies have summarized evaluation indices for assessing the efficacy of RFA ex vivo, including the ellipticity index (EI) and the regularity index (RI).

$$EI = \frac{2AD}{TD_{\max} + TD_{\min}} \tag{4.8}$$

$$RI = \frac{R_{\min}}{R_{\max}} \tag{4.9}$$

These parameters are measured within the ablated tissue, where an EI and RI value of 1 represents the standard sphere. The axial plane is defined as the plane aligned with the electrode axis (**Figure 5B**), while the transverse plane is perpendicular to the electrode and possesses the largest transverse diameter (**Figure 5C**). Maximum transverse diameter corresponds to

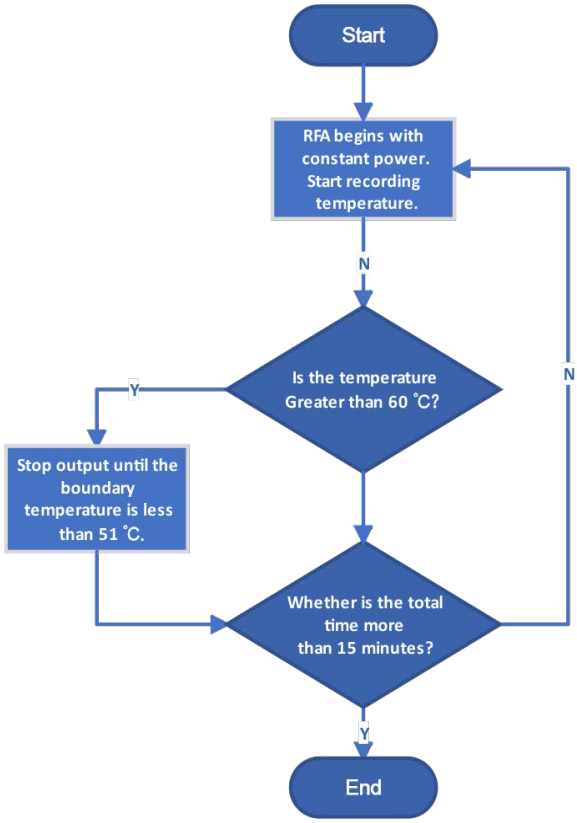

Figure 4. Flow chart of the control algorithm. RFA, radiofrequency ablation.

the maximum distance between two opposing edges, whereas minimum transverse diameter signifies the minimum distance between the edges along a relative unit in millimeters. Half of the maximum transverse diameter line is used as an intersection for measurement. AD denotes the distance between the proximal and distal edges of the coagulation zone within the axial plane along the electrode axis. Maximum radius represents the maximum distance between the edge of the solidified zone and the electrode axis within the horizontal plane. Conversely, minimum radius corresponds to the minimum distance between the edge of the solidified zone and the electrode axis within the horizontal plane (**Figure 5D**) [23].

Statistical analysis

For statistical analysis, we utilized deviation analysis simulation to compare the tissue damage diameter differences across various models. Deviation, mean value, and variance were applied to analyze the EI and RI values of the ablation range under temperature control. Deviation assessed the discrepancies between the EI and RI values and the standard values, while mean value gauged the central tendency of the RI and EI variance quantified the dispersion of EI and RI index around the mean.

Results

The simulation results of CRFA and temperature-controlled CRFA were compared

To preliminarily verify the feasibility of the temperature-controlled mode, a series of simulations were conducted to evaluate the experimental effects of CRFA in different ablation modes. Two modes of CRFA, namely cooling constant power RFA and boundary temperature-controlled CRFA, were simulated to assess their ablation effects. In the constant power mode, an active electrode length of 10 mm was employed with a continuous power output of 900 s, while the tumor diameter was set at 30 mm. To explore the feasibility of temperature-controlled CRFA, temperature control was incorporated into the CRFA simulation. The geometry of the temperature-controlled CRFA simulation model mirrored that of the CRFA, and the heat source electrodes played a consistent role.

During the simulation process, the algorithm monitored the temperature at the boundary of the tumor. When the boundary temperature exceeded 60 °C, the energy output from the electrode was paused until the temperature dropped below 51 °C, after which the energy output was resumed.

$$ONOFF = \begin{cases} 1 & T < 51℃ \\ 0 & T > 60℃ \end{cases} \quad (1.1)$$

$$V = V(T) \times ONOFF \quad (1.2)$$

During the simulation procedure, the discrete state ON/OFF of the voltage was determined by monitoring the temperature at the boundary of the tumor. The voltage output of the active electrode, denoted as V(T), represented the heat source for the actual ablation process. In the CRFA simulation, the formula $V(T) = \sqrt{(P \times R(T))}$ was employed when the power was set to a specific value. The active electrode was configured as a temperature-dependent voltage source. The ablation outcomes are presented in **Figure 6**.

Experimental results of temperature-controlled CRFA

Figure 7 depicts the ex vivo bovine liver experiment incorporating the temperature control algorithm. Following ablation, the bovine liver specimens were dissected along the electrode

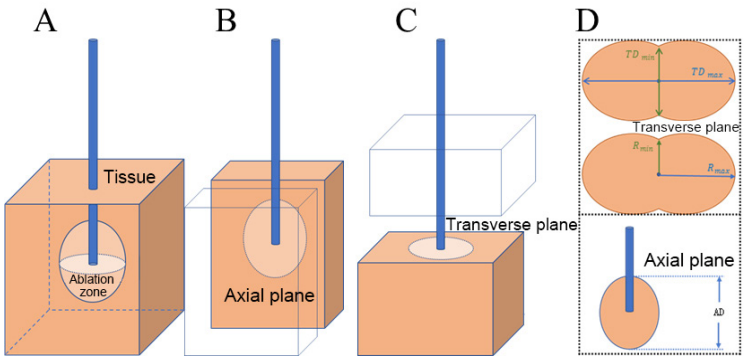

Figure 5. Schematic diagram of the ablation range. (A) Overall tissue; (B) Axial plane; (C) Transverse plane; (D) Parameters of the ex vivo experiment. TD_{max}, maximum transverse diameter; TD_{min}, minimum transverse diameter; AD, axial diameter.

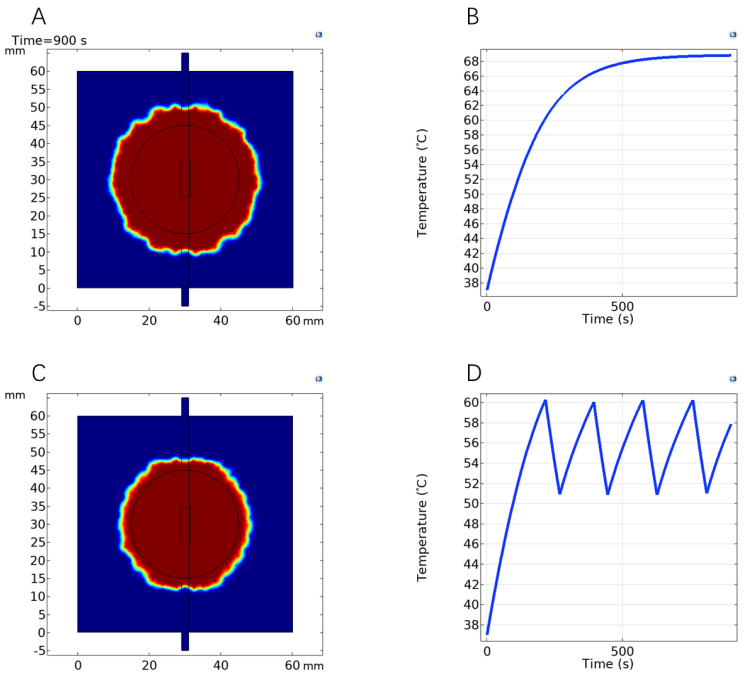

Figure 6. Simulation results of CRFA and boundary temperature-controlled CRFA. (A) Proportion of necrotic tissue in CRFA; (B) Tumor boundary temperature in CRFA; (C) Proportion of necrotic tissue in boundary temperature-controlled CRFA; (D) Tumor boundary temperature in boundary temperature-controlled CRFA. CRFA, cooling radiofrequency ablation.

needle axis, and the discolored region resulting from the ablation was quantified using a vernier caliper.

A vernier caliper was used to measure the results temperature-controlled CRFA, including the maximum transverse diameter, the minimum transverse diameter, the axial diameter, the maximum radius, and the minimum radius. **Table 2** shows the measured parameters in the discolored area in temperature-controlled CRFA.

Discussion

This study comparatively analyzed the simulation results between CRFA and temperature-controlled CRFA. During the simulation, a consistent output power of 35W was employed across all cases. **Figure 6** presents the simulation results, revealing that both CRFA and temperature-controlled CRFA achieved similar uniformity and regularity in the ablation range, surpassing the tumor boundary. The simulation results demonstrated that CRFA with the cumulative damage integral of 1 yielded ablation diameters of 43 mm, while under temperature control, the diameter reduced to 33 mm. Therefore, the extent of tissue damage was significantly reduced in temperature-controlled CRFA compared to CRFA. Under the temperature control algorithm, the temperature at the tumor tissue boundary fluctuated within the range of 50 °C to 60 °C, thereby preventing over ablation caused by excessive heating. This indicates that the theoretical control of the CRFA range under boundary temperature control is able to achieve favorable outcomes, which provides valuable guidance for ex vivo experiments.

Table 2 presents the data of various parameters related to the discolored area from temperature-controlled CRFA. Through verification via ex vivo experiments, it was observed that the diameter size of the ablation region was approximately 30 mm. In comparison to the standard spherical coagulation zone (with EI and RI both equal to 1), the maximum deviation of the EI for the traditional constant power CRFA discolored area was 7%, while the maximum deviation of the RI was 17%. The average EI was measured as 0.96, and the average RI was 0.86. The RI of the ablation results in this study is close to that of other CRFA ex vivo experiments, and the EI of the ablation range in this study is closer to the standard value than that of other CRFA, which indicates the superior performance of temperature controlled CRFA in EI [24-26]. This disparity can be attributed to the fact that the electrode surface temperature was consistently maintained below 20 °C, effectively reducing

Figure 7. Experimental plots of five groups of boundary temperature-controlled ex vivo bovine livers. (A) The axial plane of the first ablation region; (B) The transverse plane of the first ablation area; (C) The axial plane of the second ablation area; (D) The transverse plane of the second ablation area; (E) The axial plane of the third ablation region; (F) The transverse plane of the third ablation area; (G) The axial plane of the fourth ablation area; (H) The transverse plane of the fourth ablation area; (I) The axial plane of the fifth ablation region; (J) The transverse plane of the fifth ablation area.

the temperature of the surrounding tissue and mitigating the risk of excessive heating. The active cooling of the ablation electrode facilitates the delivery of higher energy to the target tissue, resulting in more effective ablation [27, 28]. The boundary temperature control regulates the output of radiofrequency energy, ensuring that the temperature at the boundary

Table 2. Parameters of the discoloration area during boundary temperature-controlled CRFA

Group	TD_{max}/mm	TD_{min}/mm	AD/mm	R_{max}/mm	R_{min}/mm	EI	RI
1	34.98	30.14	31.10	16.00	13.98	0.96	0.87
2	32.02	30.12	30.62	17.10	14.90	0.99	0.87
3	31.45	30.28	30.12	16.85	14.52	0.98	0.86
4	30.71	31.97	29.20	16.50	14.00	0.93	0.85
5	31.08	32.82	30.96	18.00	15.01	0.97	0.83

Notes: CRFA, cooling radiofrequency ablation; Td_{max}, maximum transverse diameter; Td_{min}, minimum transverse diameter; AD, axial diameter; R_{max}, maximum radius; R_{min}, minimum radius; EI, ellipticity index; RI, regularity index.

does not harm the healthy tissues surrounding it.

To conclude, in this boundary temperature-controlled CRFA, the maximum deviation between the EI and RI was minimal, with the mean value approaching a unity. Additionally, the variance values of the EI and RI were also small. These findings indicate that the self-designed CRFA instrument, coupled with the developed algorithm, enables stable control of CRFA, yielding spherical ablation patterns with a high degree of regularity. This allows doctors to better predict and plan the ablation range in clinical applications, and at the same time, the boundary temperature of the ablation area meets the condition of cell necrosis, which can ensure cell necrosis in the ablation area. The limitations of this study mainly lie in the inability to entirely replicate real-life conditions and dynamic changes, as well as the inability to obtain real-time biofeedback information, which may limit its accuracy and reliability in clinical application. Therefore, the results of ex vivo trials and clinical practice need to be considered comprehensively when evaluating RFA techniques. Despite the absence of clinical data validation analysis in this study, the ex vivo experiments exhibited promising outcomes. These findings offer a prospective avenue for further exploration and advancement of RFA in future research endeavors.

Conclusion

In this study, we initially established a simulation model using an ex vivo bovine liver model to preliminarily validate the efficacy of the boundary temperature control algorithm, which was designed to ensure the therapeutic effect while minimize unnecessary thermal damage. Subsequently, we successfully constructed the hardware platform for cooling the CRFA device following the design requirements. Finally, we conducted an ex vivo experiment to validate the results under the designed temperature control algorithm. Following the verification of the ex vivo experiment, the ablation region exhibited a diameter of approximately 30 mm, and the resulting spherical damage was stable and well-controlled. The high consistency observed between the ex vivo experiment and the simulation model results indicates the foreseeable capability of the simulation model. Furthermore, boundary temperature-controlled CRFA demonstrates improved potential for precise ablation, which establishes a foundation for further research and clinical applications, thus offering significant prospects in the field of tumor treatment.

References

[1] Cao W, Chen HD, Yu YW, et al. Changing profiles of cancer burden worldwide and in China: a secondary analysis of the global cancer statistics 2020. Chin Med J (Engl) 2021;134(7):783-791.

[2] Tatli S, Tapan U, Morrison PR, et al. Radiofrequency ablation: technique and clinical applications. Diagn Interv Radiol 2012;18(5):508-516.

[3] Habibi M, Berger RD, Calkins H. Radiofrequency ablation: technological trends, challenges, and opportunities. Europace 2021;23(4):511-519.

[4] Ni Y, Mulier S, Miao Y, et al. A review of the general aspects of radiofrequency ablation. Abdom Imaging 2005;30(4):381-400.

[5] Nath S, Lynch C, Whayne JG, et al. Cellular electrophysiological effects of hyperthermia on isolated guinea pig papillary muscle. Implications for catheter ablation. Circulation 1993;88(4 Pt 1):1826-1831.

[6] Chen MH, Yang W, Yan K, et al. Large liver tumors: protocol for radiofrequency ablation and its clinical application in 110 patients--mathematic model, overlapping mode, and electrode placement process. Radiology 2004;232(1):260-271.

[7] Taneja T, Huang S. Irrigated and Cooled-Tip Radiofrequency Catheter Ablation. 2019. p. 27-38.e23.

[8] Taneja T, Shoei K, Stephen H. Irrigated and Cooled-Tip Radiofrequency Catheter Ablation. Catheter Ablation Card Arrhythmias 2019.

[9] Cedeno DL, Vallejo A, Kelley CA, et al. Comparisons of Lesion Volumes and Shapes

Produced by a Radiofrequency System with a Cooled, a Protruding, or a Monopolar Probe. Pain Physician 2017;20(6):e915-e922.
[10] Zheng DP, Zhu MR, Liu WB, et al. Cool-tip Radiofrequency Ablation Therapy Instrument Based on Impedance Control Algorithm. J Biomed Eng 2015;32(04):905-909.
[11] Hamza NH. On the cooling effect of flowing blood on hepatic tumor ablation process. J Med Eng Technol 2018;42(6):475-481.
[12] Wang X, Gao H, Wu S, et al. RF ablation thermal simulation model: Parameter sensitivity analysis. Technol Health Care 2018;26(S1):179-192.
[13] Chang IA, Nguyen UD. Thermal modeling of lesion growth with radiofrequency ablation devices. Biomed Eng Online 2004;3(1):27.
[14] Trujillo M, Berjano E. Review of the mathematical functions used to model the temperature dependence of electrical and thermal conductivities of biological tissue in radiofrequency ablation. Int J Hyperthermia 2013;29(6):590-597.
[15] Nguyen DM, Andersen T, Qian P, et al. Electrical Impedance Tomography for monitoring cardiac radiofrequency ablation: a scoping review of an emerging technology. Med Eng Phys 2020;84:36-50.
[16] Chang I. Finite element analysis of hepatic radiofrequency ablation probes using temperature-dependent electrical conductivity. Biomed Eng Online 2003;2:12.
[17] Zhang B, Moser MA, Zhang EM, et al. A review of radiofrequency ablation: Large target tissue necrosis and mathematical modelling. Phys Med 2016;32(8):961-971.
[18] Chen XZ, Ma QY, Yang L, et al. Temperature Dependent Electrical Impedance Characteristics for Porcine Liver in Vitro. J Nanjing Norm Univ (Nat Sci Ed) 2012;35(02):32-38.
[19] Crocetti L, de Baére T, Pereira PL, et al. CIRSE Standards of Practice on Thermal Ablation of Liver Tumours. Cardiovasc Intervent Radiol 2020;43(7):951-962.
[20] Lencioni R, Crocetti L, Cioni D, et al. Percutaneous radiofrequency ablation of hepatic colorectal metastases: technique, indications, results, and new promises. Invest Radiol 2004;39(11):689-697.
[21] Venkatesan AM, Gervais DA, Mueller PR. Percutaneous radiofrequency thermal ablation of primary and metastatic hepatic tumors: current concepts and review of the literature. Semin Intervent Radiol 2006;23(1):73-84.
[22] Ng KK, Lam CM, Poon RT, et al. Porcine liver: morphologic characteristics and cell viability at experimental radiofrequency ablation with internally cooled electrodes. Radiology 2005;235(2):478-486.
[23] Mulier S, Ni Y, Frich L, et al. Experimental and clinical radiofrequency ablation: proposal for standardized description of coagulation size and geometry. Ann Surg Oncol 2007;14(4):1381-1396.
[24] Zhou W, Liang M, Pan H, et al. Comparison of ablation zones among different tissues using 2450-MHz cooled-shaft microwave antenna: results in ex vivo porcine models. PLoS One 2013;8(8):e71873.
[25] Rempp H, Mezger D, Voigtlaender M, et al. A comparison of internally water-perfused and cryogenically cooled monopolar and bipolar radiofrequency applicators in ex vivo liver samples. Acad Radiol 2014;21(5):661-666.
[26] Sommer CM, Bryant M, Kortes N, et al. Microwave ablation in porcine livers applying 5-minute protocols: influence of deployed energy on extent and shape of coagulation. J Vasc Interv Radiol 2012;23(12):1692-1699.
[27] d'Avila A, Houghtaling C, Gutierrez P, et al. Catheter ablation of ventricular epicardial tissue: a comparison of standard and cooled-tip radiofrequency energy. Circulation 2004;109(19):2363-2369.
[28] Kapural L, Deering JP. A technological overview of cooled radiofrequency ablation and its effectiveness in the management of chronic knee pain. Pain Manag 2020;10(3):133-140.